CFD MODELLING OF BLOOD FLOW IN PORTAL VEIN HYPERTENSION WITH AND WITHOUT THROMBOSIS

Svetla PETKOVA, Alamgir HOSSAIN, Jamal NASER, and Enzo PALOMBO

School of Engineering and Science, Swinburne University of Technology, Victoria 3122, AUSTRALIA

ABSTRACT

In this study we have examined blood flow in a model of the portal vein with and without obstructions to simulate conditions, which are common in liver diseases. We evaluated the impact of both conditions on the flow behaviour and found significant differences in the two models. Blockages, even when the flow conditions did not change, had an impact on the velocity magnitude, pressure, strain rate and shear stress in a model of portal vein hypertension due to liver diseases.

NOMENCLATURE

k	consistency index
u	velocity
τ	shear stress
μ	viscosity

INTRODUCTION

Portal hypertension is one of the major complications in patients with diseases of the liver, such as liver cirrhosis, veno-occlusive disease, idiopathic extrahepatic portal vein obstruction and pre-hepatic portal idiopathic pathology. Portal hypertension is a build up pressure in the portal vein, usually just before it enters the liver. Thus, there is a significant reduction of the blood flow to the liver, which causes diminished blood supply to the liver and reduction of normal liver function.

In this study we have used CFD to examine blood flow in a model of portal vein hypertension. We have compared flow with idealized thrombosis and without thrombosis, with the expectation that blockages would affect blood flow.

MODEL DESCRIPTION

Flow model

We have used a simple 3D geometry, shown in figures 1 and 2, which has 4 branches with different flow rates. Table 1 shows the dimensions of the geometry used in this model. At inlet (bottom) the velocity is considered to be 0.07 m/s and operating pressure is 3922.66 Pascal according to J-P.TASU (2002). The velocity magnitude, pressure, and dimensions of the geometry are an approximation from the majority of published values. This model geometry was constructed by using Gambit 2.0.4 (FLUENT 6.0) with tetrahedral and hexahedral grids shown in figures 1 and 2. Figure 1 is the simple portal vein

with no blockages and figure 2 has a few blockages: one in at the main vein and other two are in first main branches. The number of computational grid cells for figure 1 is 27,457 and 60,731 for figure 2. The simulations were carried out using a super computer at VPAC (Victorian Partnership of Advanced Computing), which takes up to 60 minutes to converge using Fluent 6.0. The flow properties of blood used in this study are given in table-2 (Syoten Oka, 1980). The convergence criterion of reduction of residuals by five orders of magnitude for continuity and three orders of magnitude for other transport equations was used.
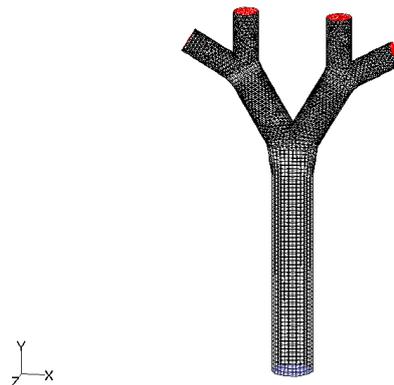
Figure 1: Portal vein with 4 branches (27,457 grids).
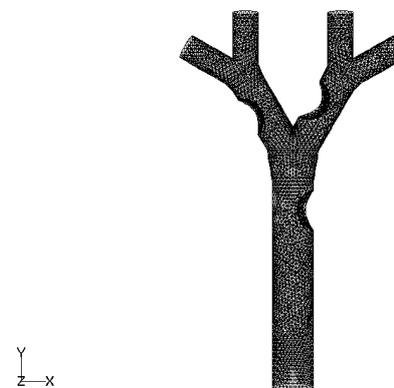
Figure 2: Partially blocked Portal vein with 4 branches (60,731 grids).

Table 1: Model dimensions

Inlet diameter	10 mm
First branching diameter	8.5 mm
Outlet diameter	6.375 mm
Total hight of the	91 mm

Table 2: Non-Newtonian power law parameters (see equation 8):

Power law index (n)	0.4851
Consistency index k (kg-s^n-2/m)	0.2073
Reference temperature (^{0}K)	310
Minimum viscosity limit η_{max} (kg/m-s)	0.00125
Maximum viscosity limit η_{min} (kg/m-s)	0.003

This paper describes the non-Newtonian simulations only. The simulation for Newtonian flow, not shown in this paper, shows minor changes in the results around the obstacles.

MATHEMATICAL MODEL

Continuity and Momentum Equations

For all flows, FLUENT solves conservation equations for mass and momentum. For flows involving heat transfer or compressibility, an additional equation for energy conservation is solved. For flows involving species mixing or reactions, species conservation equations are solved or, if the non-premixed combustion model is used, conservation equations for the mixture fraction and its variance are solved. Additional transport equations are also solved when the flow is turbulent. In this paper, the conservation equations for laminar flow (in an inertial, non-accelerating, reference frame) are presented

The Mass Conservation Equation

The equation for conservation of mass, or continuity equation, can be written as follows:

$$\frac{\partial \rho}{\partial t} + \nabla \cdot (\rho \vec{v}) = S_m \tag{1}$$

Equation (1) is the general form of the mass conservation equation and is valid for incompressible as well as compressible flows. The source S_m is the mass added to the continuous phase from the dispersed second phase (e.g., due to vaporization of liquid droplets) and any user-defined sources. In this case it is 0.

Momentum Conservation Equations

Conservation of momentum in an inertial (non-accelerating) reference frame is described by

$$\frac{\partial}{\partial t}(\rho \vec{v}) + \nabla \cdot (\rho \vec{v} \vec{v}) = -\nabla p + \nabla \cdot (\overline{\tau}) + \rho \vec{g} + \vec{F} \tag{2}$$

where p is the static pressure, $\overline{\tau}$ is the stress tensor (described below), and $\rho \vec{g}$ and $\vec{F}$ are the gravitational body force and external body forces respectively.

The stress tensor $\overline{\tau}$ is given by

$$\overline{\tau} = \mu \left[\left(\nabla \vec{v} + \nabla \vec{v}^T \right) - \frac{2}{3} \nabla \cdot \vec{v} I \right] \tag{3}$$

where μ is the molecular viscosity, I is the unit tensor, and the second term on the right hand side is the effect of volume dilation.

Viscosity for Non-Newtonian Fluids

For incompressible Newtonian fluids, the shear stress is proportional to the rate-of-deformation tensor $\overline{D}$:

$$\overline{\tau} = \mu \overline{D} \tag{4}$$

where $\overline{D}$ is defined by

$$\overline{D} = \left(\frac{\partial u_j}{\partial x_i} + \frac{\partial u_i}{\partial x_j} \right) \tag{5}$$

and μ is the viscosity, which is independent of $\overline{D}$. For some non-Newtonian fluids, the shear stress can similarly be written in terms of a non-Newtonian viscosity η:

$$\overline{\tau} = \eta (\overline{D}) \overline{D} \tag{6}$$

In general, η is a function of all three invariants of the rate-of-deformation tensor $\overline{D}$. However, in the non-Newtonian models available in FLUENT, η is considered to be a function of the shear rate $\dot{\gamma}$ only. $\dot{\gamma}$ is related to the second invariant of $\overline{D}$ and is defined as

$$\dot{\gamma} = \sqrt{\overline{D} : \overline{D}} \tag{7}$$

FLUENT provides four options for modelling non-Newtonian flows:

- Power law
- Carreau model for pseudo-plastics
- Cross model
- Herschel-Bulkley model for Bingham plastics

Note that the non-Newtonian power law described below which has been used in this model.

Power Law for Non-Newtonian Viscosity

The non-Newtonian-power-law model is used in this study, where the non-Newtonian viscosity is calculated as (FLUENT 6.0 Manual, Chapter 7.3.5):

$$\eta = k \dot{\gamma}^{n-1} e^{T_0/T} \tag{8}$$

FLUENT allows upper and lower limits to be placed on the power law function, yielding the following equation:

$$\eta_{min} < \eta = k \dot{\gamma}^{n-1} e^{T_0/T} < \eta_{max} \tag{9}$$

where k, n, T_0, η_{min}, and η_{max} are input parameters. k is a measure of the average viscosity of the fluid (the consistency index); n is a measure of the deviation of the fluid from Newtonian (the power-law index), as described below; T_0 is the reference temperature; and η_{min} and η_{max} are, respectively, the lower and upper limits of non-Newtonian viscosity used in the power law. If the viscosity computed from the power law is less than η_{min}, the value of η_{min} will be used instead. Similarly, if the computed viscosity is greater than η_{max}, the value of η_{max} will be used instead. Table 2 shows how viscosity is limited by η_{min} and η_{max} at low and high shear rates in this model. The value of n determines the class of the fluid:

- n = 1 → Newtonian fluid
- n > 1 → shear-thickening (dilatant fluids)
- n < 1 → shear-thinning (pseudo-plastics)

The values of k and n used in this study were obtained from data of shear rate vs shear stress (Syoten Oka, 1980).

RESULTS

The outflow was pre-defined with flow rate weighting 0.15 for each of outlets 1 and 2 (left branch) and 0.35 for each of outlets 3 and 4 (right branch). In both models the same parameters were used (see above) and the following results were obtained (Fig 3-6). We use the differentiation

of the flow rate in the outlets based on the fact that the two lobes of the liver are different in size (the left lobe is over 2 times smaller than the right one).
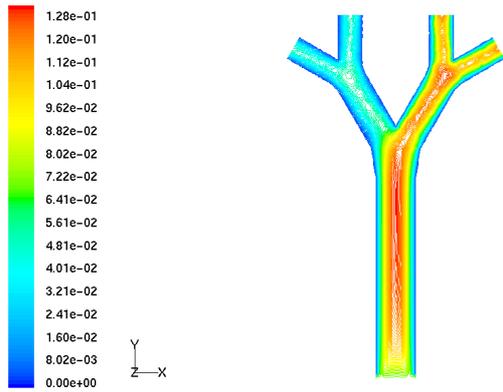
Figures 3a: Contour of velocity magnitude on an x-y plane cutting through the middle of the geometry without blockages.
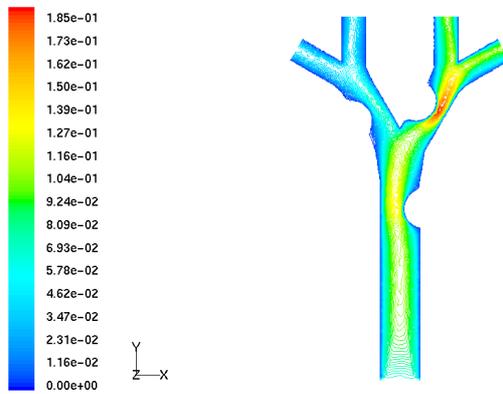
Figures 3b: Contour of velocity magnitude on an x-y plane cutting through the middle of the geometry with blockages.
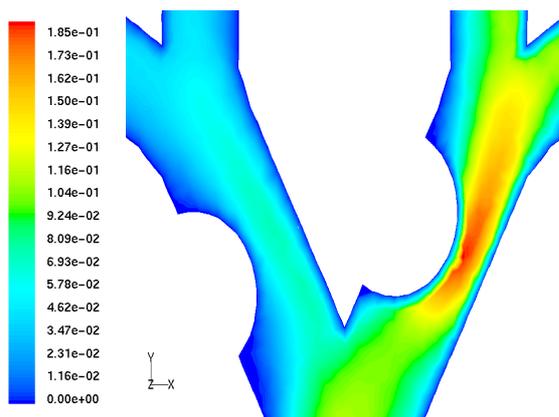
Figure 3c: Closer view contour of velocity magnitude on an x-y plane cutting through the middle of the geometry with blockages.

Figures 3a and 3b show velocity contours on an x-y plane cutting through the middle of the geometry (see figure 1). Figure 3c also represents the velocity contour near blockages. As can be seen from figures 3a and 3b, there were significant changes in the velocity magnitude in the

two conditions. The way the model was created assumed that the problem causing portal hypertension was in the liver, the portal venous flow was diminished and the portal vein pressure was 3922.66 Pascal (40 cm H_2O). In this case there are two possible conditions: Figure 3a shows the velocity magnitude if there were no additional complications in the portal vein; Figure 3b shows the additional complication of portal vein thrombosis and the impact on blood flow. Near blockages velocity is very high (figure 3c) and thereby the pressure is low. This may cause of more shrinkage of vein, which stops blood circulation finally. In this model, there is no additional decrease in velocity, and so it gives the most favourable picture of this condition (i.e. hypertension).

Figures 4a and 4b show pressure contours on an x-y plane cutting through the middle of the geometry (see figure 1). These two figures correlate to the findings of figures 3a and 3b. The zones of low pressure, which were typical for the two higher flow outlets (figures 4a and 4b), have "moved" to the area of the blockages, thus increasing the pressure in the low flow outlets (figure 4b).
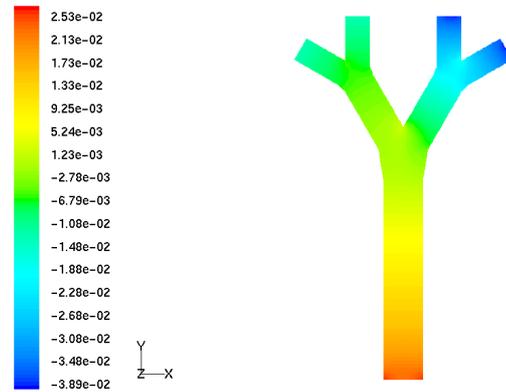
Figures 4a: Contour of static pressure on an x-y plane cutting through the middle of the geometry without blockages
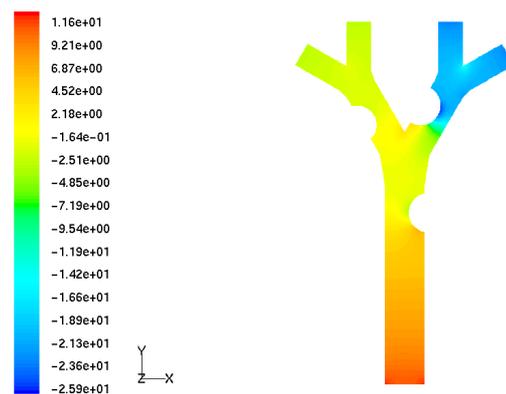
Figures 4b: Contour of static pressure on an x-y plane cutting through the middle of the geometry with blockages

Figures 5a and 5b represent the contour of strain rate on an x-y plane cutting through the middle of the portal vein (see figure 1). In figure 5a the strain rate is uniform through the portal veins according to the velocity distribution. But in figure 5b the contour of strain rate is not uniform because of the existence of obstacles in blood flow. As expected

the strain rates are higher in the constriction created by the obstruction.
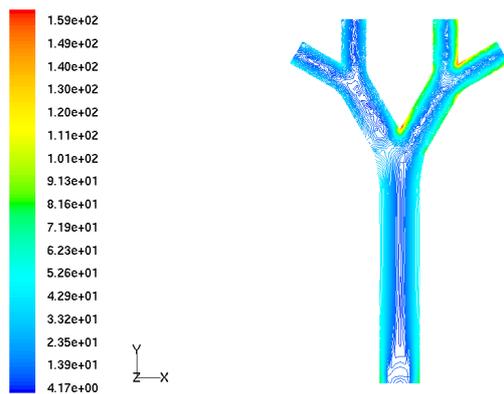
Figures 5a: Contour of strain rate on an x-y plane cutting through the middle of the geometry without blockages.
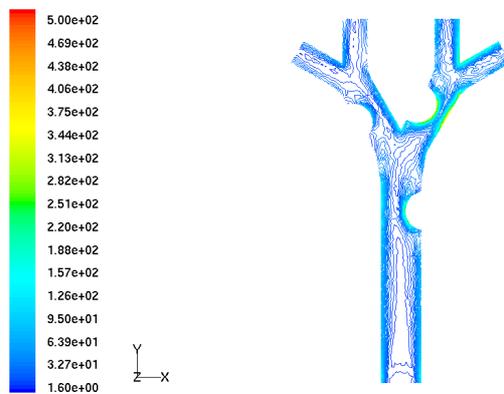
Figures 5b: Contour of strain rate on an x-y plane cutting through the middle of the geometry with blockages
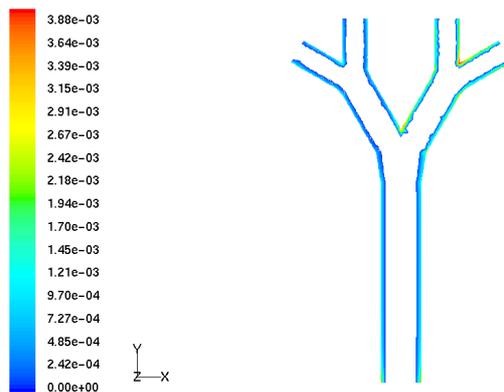
Figures 6a: Contour of wall shear stress on an x-y plane cutting through the middle of the geometry without blockages.

Figures 6a and 6b show contour of wall shear stress near the wall on an x-y plane cutting through the middle of the geometry (see figure 1). The blockages in the portal veins decrease the available cross section area. This reduction of available cross section area ultimately introduces higher strain rates around the blockages. The higher strain rates around the blockages results in significantly higher shear stress near the wall presented in figure 6b. The portal veins without blockages in figures 5a and 6a show much lower values of strain rates and wall shear stress.
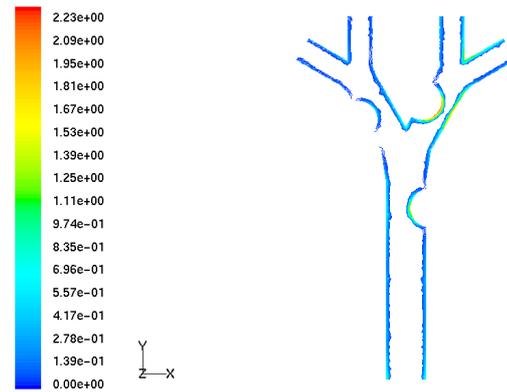
Figures 6b: Contour of wall shear stress on an x-y plane cutting through the middle of the geometry with blockages

CONCLUSION

These simulations confirmed the expectation that the blockages would have an effect on the blood flow in the portal vein even in the case of diminished blood supply to the liver due to disease of the organ. We have used low flow velocity, although increased compared to normal portal vein and average pressure of 40 cm H_2O column. The clinical condition our presentation is based on is portal hypertension and we examined the impact of blockages on this condition. The next study will be based on the size and location of the blockages and their impact on the flow to the liver under the same conditions. We will add to the model the thrombogenic effect of the blood in portal hypertension with blockages. The input data to this CFD model can be from *in vivo* measurements (Duplex Ultrasound, Magnetic Resonance, echo-Doppler, Doppler Duplex sonography, Biopsy and other) for individual patients. This model can be adjusted for a variety of flow parameters and can assist medical practitioners, in conjunction with the patient-based measurements, to predict the degree of risk to the patient. We believe that this type of model can be used to predict the chances of survival and the risks of liver failure and mortality in patients with portal hypertension.

REFERENCES

SYOTEN OKA (1980), "Cardiovascular Hemorheology" , *Cambridge University Press*

ANDREAS OCHS, MD, at al (1995), "The Transjugular Intrahepatic Portosystemic Stent-Shunt Procedure for Refractory Ascites", *New England Journal of Medicine* 1995; 332: 1192-1197

J-P.TASU, at al,(2002), "Hepatic Venous Pressure Gradients Measured by Duplex Ultrasound", *Clinical Radiology* (2002) 57:746-752

YANG-YAO NIU, et al, (2002), "Numerical Simulations of Aortic Flow Problems Based on A Parallelized Artificial Compressibility Solver", *Proceedings.of the Secound International Conference on Computational Fluid Dynamics*, ICCFD, Sydney, Australia, 15-19 July 2002.